9

Ultrafast Photoluminescence in Nanowires

Zhao FL[1], Wang XF[1,4], Chen HJ[1,2] and Luo JY[1,3]
[1]*Sun Yat-sen University*
[2]*The Chinese University of Hongkong*
[3]*Wuyi University*
[4]*Guangdong University of Petrochemical Technology*
China

1. Introduction

As the boundary condition was dropped down to the nanometer scale, the photo electronic properties can be changed dramatically especially that the photon luminescence (PL) properties may be changed significantly. Because two of the dimensions is comparable to or even smaller than the wavelengths of the PL, the nanowires are expected to show a variety of quantum confinement effects, such as density of state singularities, macro molecular behaviour over the long distances, high coherence of the emission, much high luminescence efficiency and low lasing threshold which is essential to construct novel integrated photo electronic devices in nanoscale. Besides, the high surface-to-volume ratio of these nanostructures also allows studying the role of surface states (and their ambient-driven changes) in determining the nanostructure carrier transport and optical excitation/recombination properties. The surface state and quantum confinement are two fundamental effects responsible to the photo electronic characteristic of nanostructures. Naturally the photoelectronic properties determine the future application for nanostructures including nanoparticles, nanowires, nanorods and so on. For example photo electronic properties determine whether the nanowires fabricated are suitable for such electronic application as field emission and photo-detection etc. Meanwhile many kinds of nanowires whose bulk materials can be used as photo luminescent sources are taken granted as the nanolaser active media. Such an idea needs lots of experiment to examine and confirm by the data of both the steady-state spectroscopy and time-resolved spectroscopy dynamically.

Therefore we demonstrate a series studies on dynamic mechanism of nanowires (1 dimensional structure) and nanoparticles (0 dimensional structures) with respect to time, excitation density and photonic energy of PL. The sample focused are zinc oxide (ZnO)(Wang et al., 2009), carbon silicon (SiC)(Zhao et al., 2007), tungsten oxide (WO) covering both direct bandgap semiconductor and indirect bandgap semiconductors.

The following will present the surface state effect on nanoparticles, ultrafast light emission from nanowires and directional lasing behaviour from nanotree. The mechanism of the ultrafast light emission will be discussed qualitatively.

2. Experimental method

The ultrafast photoluminescence experiment demonstration was constructed with laser system, sample adjustment and detection system. The laser system was select based on the steady state PL spectroscopy of the nanowires. For example, we selected the femtosecond laser pulse at wavelength of 320nm to study the band-band transition of SiC nanowires and ZnO nanoparticles. But for the surface-state exploration we chose picosecond laser pulse at wavelength of 532nm for excitation to the ZnO nanosparticles and we selected picosecond laser pulse at wavelength of 300nm for the excitation to the nanodiamond particles(Zhao et al., 2004). The sample design includes the direction alignment of the sample, the consideration of the polarization of the excitation and the detection because the nanowires undergoes special orientation which is sensitive to the excitation polarization and gives light emission in certain direction and polarization. If necessary we would arrange for a set of microscope monitor system to infirm the correct excitation locally.The detection system was constructed by a set of selective streak cameras and the corresponding spectroscope. The streak camera can be changed with the different time-resolution from 20 picosecond to 700 femtosecond. The spectroscope can be selected whether the quartz prism spectroscope was used for ultraviolet detection for the high transmissivity or the optical grating spectroscope for high wavelength resolution was applied for the proper spectral limit.

2.1 Experiment set-up

The experimental set-up is shown in Figure 1. The laser system includes commercial available femtosecond laser system with optical parameter amplifier (OPA), picosecond

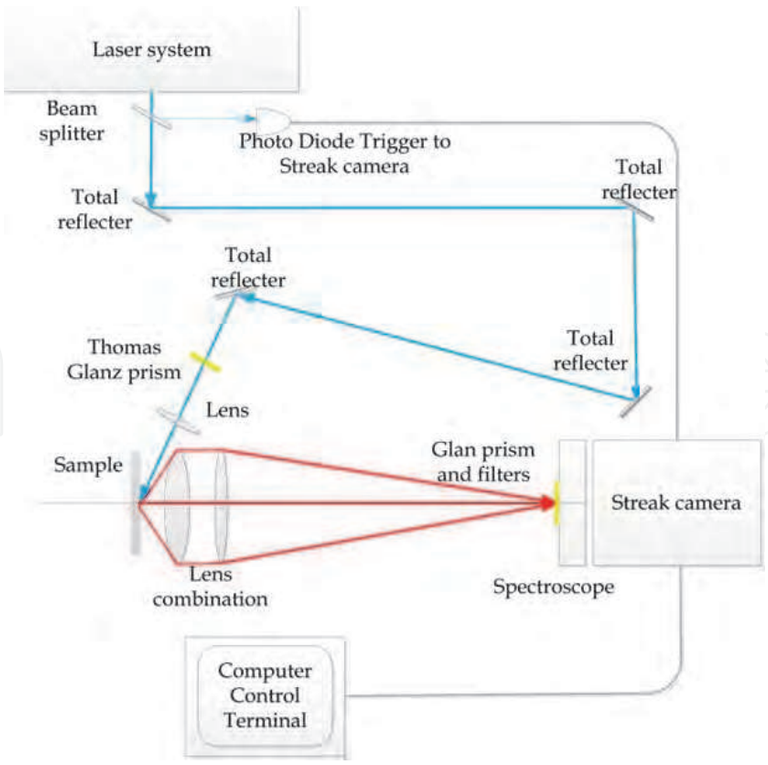

Fig. 1. Experimental set-up for ultrafast photoluminescence measurement

laser system with Cavity-damped dye laser and high energy picosecond laser system with OPA. Different laser sources are selected due to different motivations. The three total reflectors are adjusted for compensate the electrical delay of the photodiode triggering the streak camera in order to keep the synchronism between the optical induced signal and the triggering signal. But for the streak camera with high repetition rate such as 82 MHz, the external optical delay path is not necessary since the laser excitation keeps constantly both on the intensity and the profile in time domain. The excitation can be focused to the sample on face or from the behind according to the properties of the sample. Generally, the excitation incidence beam is injected on face to the sample fabricated on the substrate of silicon or some other opacities. Furthermore in order to avoid the excitation light into the detection system the excitation can be assigned as perpendicular to the emission collecting lens axis especially for the colloidal solution of nanostructures. The two Glan-Laser Calcite Polarizer prisms are adjusted for the polarization selected and the intensity manipulation for excitation. Additionally the cut-off filters for the excitation can not be neglected for preventing the detection system exposed under high irradiation of the laser.

2.1 Deconvolution of the time-resolved spectroscopy

The fluorescence detected by the streakcamera is the convolution of the instrumental response function and the fluorescence of the materials. Assume the instrumental response function is $I(t)$ and the fluorescence of the materials is $F_{theo}(t)$ the detected light emission is $F_{exp}(t)$, they can be described by the equation (1).

$$F_{\exp}(t) = I \otimes F_{theo} = \int I(t) F_{theo}(t - t') dt' \tag{1}$$

Here the instrumental response function consists the excitation and the influence of the optical filters and lenses. The total influence tends to be in the distribution as Gaussian function profile in time-domain. Because the ideal transition rate at room temperature is proportional to the life-time reversely, we considered the theoretical fluorescence intensity $F_{theo}(t)$ as a sum of multi-exponential form:

Therefore we should find proper amplitude and corresponding life-time satisfying the following:

$$F_{exp}(\mathrm{t}) = \int I(t) \sum_{i=1,n} a_i exp(-t/\tau_i) \tag{2}$$

We applied an iterative Monte-Carlo method to search the best result out of the fluorescence decays with consideration of a global optimization algorithm. It should be noticed that the parameter a_i are normalized percentage and the sign of a_i implying the energy out (positive) and in (negative). Energy out means that the photons are emitted from the materials and energy in means that energy has been transferred into the materials to bring them in excited states or leading to other active states alike.

2.2 ultrafast photoluminescence from ZnO nano particles

As the so-called nanowires is quasi 1-dimensional material. The photo electronic properties may undergo both bulk-like and nanodots-like. For example the laser cavity effect is originated from the bulk materials while quantum confinement effect and surface state effect are more dependent upon the quantum dots and the nanoparticles. In order to get the

whole description of nanowires we should make it clear that the photo electronic properties of nanodots or nanoparticles.

2.2.1 Surface state induced ultrafast photoluminescence from ZnO nanoparticles

The quantum confinement effect (QCE) and surface states are two incompatible physical mechanisms in modifying the energy band structure of nanostructures. These two mechanisms compete with each other on the influence to PL spectra. For nanodots or nanostructures with diameters less than 10 nm, the QCE plays a dominant role while the large surface-to-volume ratio also brings much influence on the system's Hamiltonian when the material size is reduced to the nanometre scale. Therefore we demonstrated the size-dependent time-resolved PL spectra of ZnO nanoparticles with different sizes. The results show a key role of the surface states recombination in the PL of nanometre sized particles due to the large surface- to-volume ratio.

ZnO nanoparticles of different grain size were prepared by the homogenous precipitation method (HPM)(Wang et al., 2006). The average particle sizes for five groups of samples are 17 nm, 25 nm, 40 nm, 10 nm and 300 nm. The samples were excited by quasi-continuous picosecond (ps) laser pulses from Vanguard 2000-HM532 laser at 532 nm at room temperature. The laser pulse duration is 12 ps and the pulse repetition is 82 MHz. The maximal output laser power is 2 W. The excitation laser pulses were focused on the sample by a lens with a focal length of 75 mm. The emission was collected before being detected by a synchroscan streak camera (Hamamatsu M1587, resolution of 10 ps) for time-resolved photo luminescence (TRPL) detection. Fig. 2 gives the image of the streak camera of two kinds of nanoparticles representatively. Both images are obtained under the same spectral condition. The focused spot size of the laser beam is 100 micrometer in diameter, and the excitation power density is 2.59 $\times 10^5$ W/cm^2. All the PL spectra exhibit broad bands covering the range from 1.2 eV to 2.3 eV. From Figure 2 we can see clearly that with the increased grain size of the ZnO nanoparticles, the PL band undergoes a red-shift significantly. By optimizing the peak position and half-width of the Gaussian peaks, it was possible to obtain a good fit for the four-peak combination coming from the surface state induced light emission.

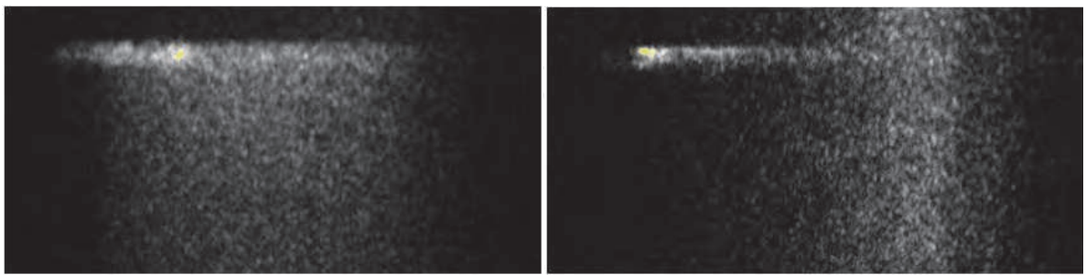

Fig. 2. The image of surface induced ultrafast light emission. (a) Particle grain size is 20nm, (b) Particle size is 300nm.

The band structure analysis are shown in table 1, Xc indicates the deconvoluted peaks according to Gaussian method with both the central position of the peak and the corresponding intensity. As labeled, the four Gaussian peaks are centered at Xc1, Xc2, Xc3, and Xc4 from the highest photonic energy to the lowest one. All the PL spectra are obtained under the same experimental condition.

Sample	Size (nm)	Xc1		Xc2		Xc3		Xc4	
		Peak (nm)	Inten. (a.u.)	Peak (nm)	Inten. (a.u.)	Peak (nm)	Inten. (a.u.)	Peak (nm)	Inten. (a.u.)
a	20	596	0.41	643	0.71	730	0.66	807	0.25
b	25	595	0.35	648	0.69	739	0.69	804	0.38
c	40	602	0.37	661	0.67	750	0.63	810	0.42
d	110	589	0.18	698	0.46	762	0.42	807	0.49
e	300	598	0.12	700	0.41	764	0.44	807	0.48

Table 1. The band structure analysis results of ultrafast light emission from nanoparticles with various grain sizes.

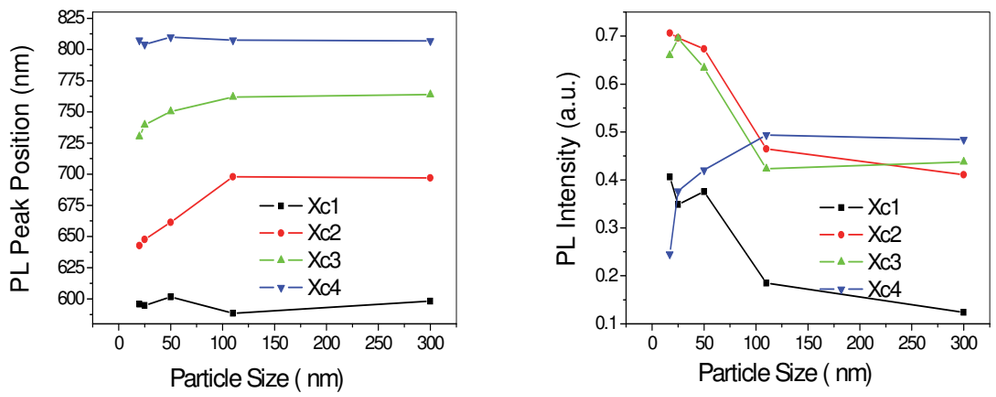

Fig. 3. The size threshold for surface-state light emission (left) relationship between the peak position and the grain sizes; (right) relationship between the PL intensity and the grain sizes.

Fig. 3 provides the luminescence peak position and the corresponding relative amplitude as a function of ZnO particle size. Upon increasing the grain size from samples ***a*** to ***e***, slight wavelength changes were observed for the Gaussian peaks denoted as Xc1 (~2.08 eV) and Xc4 (~1.54 eV), respectively. While the luminescence peaks Xc2 and Xc3 shift to lower energy as the grain size increases. The wavelength of Xc2 shifts from 1.93 eV (sample ***a***) to 1.77 eV (sample ***e***), and that of Xc3 shifts from 1.70 eV (sample ***a***) to 1.62 eV (sample ***e***). In addition, upon increasing the particle size, the relative amplitude of the Xc4 band is found to increase accordingly, while that of Xc3 band decreases. However, little change is observed for bands Xc1 and Xc2. Therefore, the Gaussian analysis indicates that the red-shift in the PL spectra is mainly the result of the increase in relative magnitude of the Gaussian combination in the lower energy region.

The energy band gap of ZnO is about 3.37 eV, corresponding to light emission at wavelength of 368 nm. ZnO luminescence mainly covers three bands: ultraviolet (UV), green and orange. Most scientists indicated that the green PL comes from intrinsic defects in ZnO samples, while the orange or yellow emission comes from lithium and other impurities (Djurisic et al., 2005). Under such a low photonic energy excitation of 2.33 eV (532nm), which is much lower than that for the band gap transition of ZnO, the PL spectra of all the nanoparticle samples clearly exhibit broad emissions in the range from 1.2 eV to 2.3 eV. The broad emission bands are not considered to come from the introduced impurities, because

no impurity was detected in our samples during identification. Such spectra indicate that certain states must lie in the fundamental energy band gap close to the Fermi level of ZnO nanoparticles. We attribute the broad bands obtained with the low photon energies to surface-state transitions, because the only difference in the preparation is the temperature corresponding to their particle sizes.

The existence of such surface-state bands has firmly been established both experimentally and theoretically. Moreover, the surface states located close to the Fermi level are due to the so-called dangling bond in elemental semiconductors. A dangling bond on a crystal surface likely gives rise to a localized state within the band gap. The unsaturated covalent bands can easily form states especially in the center of the gap. Although, it is suggested that no gap surface states exist on perfect ZnO surfaces, as no broken *sp*3 bulk bonds are present. In the case of nanoparticles, however, one of the key features is the large surface-to-volume ratio (S/V). That is, the large S/V greatly increases the possibilities of dangling bonds or broken bonds in ZnO nanoparticles, which is confirmed by our experimental results (Wang et al., 2007). Upon increasing particle size, however, the time-resolved optical emission process exhibits significant differences. For simplicity, Figure 4 shows the time decay curves of three typical different average sizes of samples ***a***, ***c*** and ***e***, with diameter of 17 nm, 40 nm and 300 nm, respectively. Upon increasing the particle diameter, the decay rate of the PL obviously slows down. With regards to the theoretical radiative recombination as a sum of exponential functions, we applied a deconvolution procedure based on the Monte-Carlo algorithm to search dynamic lifetimes. The bi-exponential decay process has been observed for samples ***a*** and ***c***. Figure 4a and Figure 4b show the corresponding fitted results, in which the scatters represent the experiment data and the solid line is the exponential fitting. The two lifetime constants of sample ***a*** are about 96 ps and 1.1 ns with relative amplitudes of 0.70 and 0.30, respectively, while those for sample ***c*** are about 190 ps and 2ns with relative amplitudes of 0.82 and 0.18, respectively. In the case of the largest particle size of sample ***e***, we cannot see the decay of the emission within the observed time scale as shown in Fig. 4c.

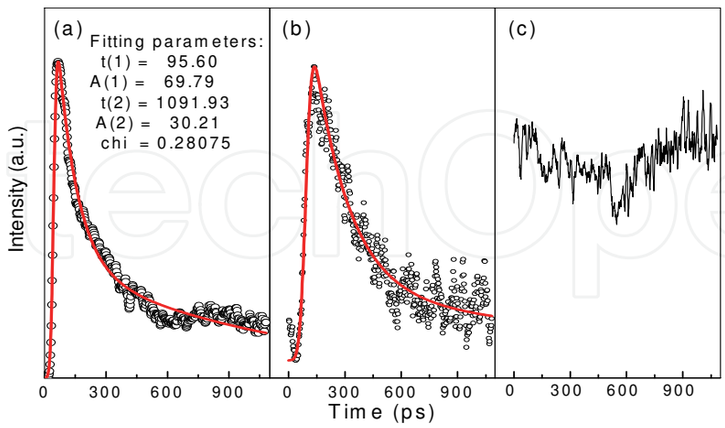

Fig. 4. The time decay curves of three typical different average sizes of samples a, c and e, with diameters 17 nm, 40 nm and 300 nm, respectively.

From our spectral results we can concluded that as the grain size is increased the surface state induce light emission turns to weak and the lifetime turns longer. It should be noted that as the grain size drops down to several nanometer the quantum confinement should be

dominant to the ultrafast light emission because the bandgap enlargement will be much strong than the disturbance induce by surface state. As the size of the grain goes up to certain value that the bulk structure becomes dominant so that the surface-volume ratio is not much significant the surface state induced light emission should be diminished. Just at a proper size region the surface-state induced light emission cannot be neglected and this may bring important effect to the photo electronic integration on nanometer scale because of the size-peak-lifetime dependent light emission.

2.2.2 Lasing effect from ZnO nanoparticles

Besides Surface state effect in nanoparticles there is other interesting lasing effect from nanoparticles of ZnO. The experiment was demonstrated at room temperature. The excitation laser pulse was generated from commercial available OPA system pumped by Ti: sapphire system (Maitai, Spectral Physics) at wavelength of 320 nm with the pulse repetition of 1 kHz. The pulse duration is 160 fs. The excitation intensity was manipulated by a Glan-Laser Calcite Polarizer-Laser Calcite Polarizer prism. The light emission was collected by a lens composition before focused into the transient spectroscopy system (HAMAMATSU C 6860) connected with quartz prism spectroscope. The spectral resolution is less than 1 nm. In spite that time-resolution is 700 fs the laser pulse was indeed broadened by optical apparatus so that the overall time-resolution of the detection system is 1ps.

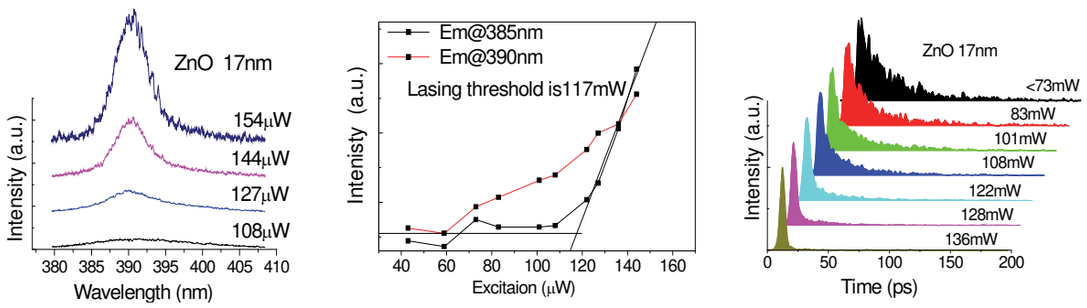

Fig. 5. The ultrafast light emission from ZnO nanoparticles.

Figure 5 shows that ultrafast lasing effect of ZnO nanoparticles with the size of about 17nm. The wavelength spectrum shows no sharp peak emerging at 385nm or at 390nm which is different from the lasing from ZnO bulk crystal materials. One reason is that electron hole plasma is generated in the nanoparticles and the nanometer boundary condition and the nanoparticles cannot provide any kinds of cavity to generate optical resonance. Furthermore the PL life time is shortened as the pump power increased until the pump power was increased to 136 micro Watt that the decay curve time-resolved PL turns to be symmetrical. Such a fast process implies that the EHP possesses an ultrafast behaviour in nanometer scale.
Therefore, surface state effects play important role in ultrafast light emission from the nanometer particles and the ultrafast light emission related to the transition from the conduction band to the valence band is rather an ultrafast lasing effect than nanolaser. Therefore nanoparticles are not proper candidates for special wavelength respected nanolaser; the nanowires may be a good choice. But the pumping intensity dependence of the PL intensity indicate that the PL at wavelength of 385nm corresponding to the band-band transition of the ideal ZnO crystal structure still under goes the linear dependence as the pumping power is above 117 micro. This is the important evidence for amplified

stimulated light emission but not laser because the no cavity has been generated for any oscillation. That is nanoparticles can build amplified light emission easily but cannot construct the oscillating cavity.

2.3 Ultrafast photoluminescence from SiC nanowires and WO nanowires

Nanoparticles are quasi zero dimensional materials and the PL spectra imply that the nanolaser cannot be respected from just the nanoparticles. Nanowire is quasi 1D material and it undergoes the photo electronic properties of both nanoparticles and the bulk one. Therefore may the nanowire be the ideal candidate for more application in photo electronic.

We have studied the ultrafast light emission of SiC nanowires and WO nanowires and we have measured the ultrafast wide band blue light emission from SiC nanowires and super fluorescence from WO nanowires. The structural characterizations of SiC nanowires and WO nanowires have been shown in the Figure 6.

The experiment of Ultrafast photoluminescence spectroscopy for nanowires of SiC and WO are carried out under femtosecond laser pulse excitation at the wavelength of 320nm from an OPA of a femtosecond (fs) Ti: Sapphire laser with pulse duration of 160 fs (commercial OPA model 800CF, Amplifier model Hurricane, Seed model Maitai from Spectra-physics). By a fused silica lens (75.6-mm focal length), the excitation pulse was focused onto the sample surface at an angle of about 45º to the normal of the surface. The average power of the excitation on the sample was about up to 400 micro Watt (corresponding to a power density of about 10 GW/cm^2).

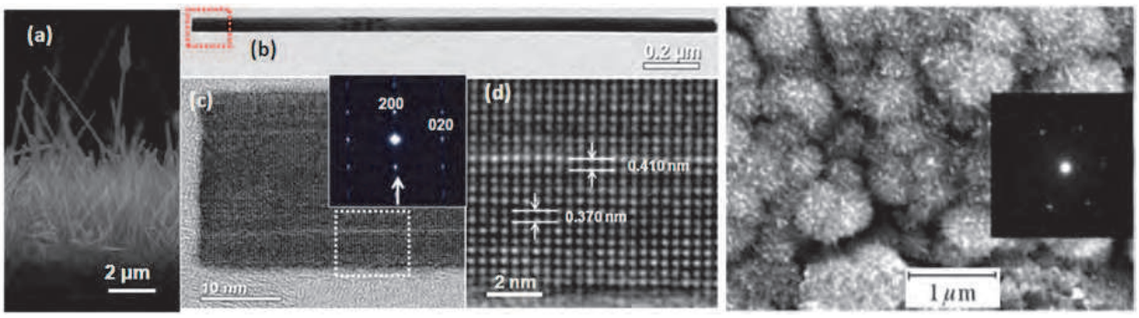

Fig. 6. Morphology of nanowires of WO and SiC, (a) is the SEM of WO nanowires, (b) (c) and (d) are the SEM, XRD and HRTEM for WO lattice characterization; (e, the right most) is the SEM and XRD characteristic of SiC nanowires.

The PL from SiC nanowires was collected at a direction normal to the sample surface and collected into the spectroscope connected with a streak camera (Hamamatsu C1587) with a time resolution of 2 ps. The temporal full-width at half- maximum (FWHM) of our instrument response function (IRF) was less than 10 ps.

For the PL from WO nanowires we can choose the spectral resolution from 0.5nm to 6.0nm and the time resolution from 10ps to less than 1ps.

2.3.1 Ultrafast light emission from SiC nanowires

The details of the spectroscopy of SiC nanowires and the powder of SiC are shown in Figure 7. The photoluminescence of SiC nanowires exhibits wide emission band and cannot be all included in the interested spectra range for the limitation of the spectrometer. From the

figure, we can see that there is a large blue shift (~29 nm) between the emission centers of SiC powder and SiC nanowires. Obviously, the blue shift is caused by the nanowires. The photoluminescence of SiC powder can be well fitted by a single Gaussian line with its peak at 446.6nm. However, the emission of SiC nanowires is much broad and represents multiple peaks. We performed Gaussian multi-peak fitting process to the deconvolution and got the result of two peaks located at 418nm and 446.6nm respectively. Thus we can conclude that the peak at 446nm is due to the emission from the SiC powder, while the wide peak at 418nm is caused by the SiC nanowires. Because the diameter of the nanowires ranges from 20 to 50 nm and the curvature of the apex of the nanowires can be down to 2 nm, there should be great difference in the degree of quantum confinement and the surface-to-volume ratio of the nanowires, which accounts for the wide emission peak of the nanowires and the slight shift of the PL peak wavelength. It is well known that the band gap of the bulk 3C SiC is 2.3 eV (Bimberg et al., 1978), corresponding to the emission at the wavelength of 539 nm at room temperature, therefore, the PL peak energy of the nanowires is blue-shifted. But such large blue shift is not practical for quantum confinement. Another reason is that the SiC nanowire undergoes certain phase transition so that 6H SiC was present in the process of the irradiation under intense femtosecond laser pulse. Even for 6H SiC material the bandgap is 2.9 eV corresponding to the light emission at wavelength of 427nm our light emission at 418nm still present a blue shift significantly which due to 64 meV of the band gap widening. Similar results have been obtained in other low-dimensional SiC, the blue-shift emission peak can be explained by the energy gap widening due to the quantum confinement effect in these nanowires.

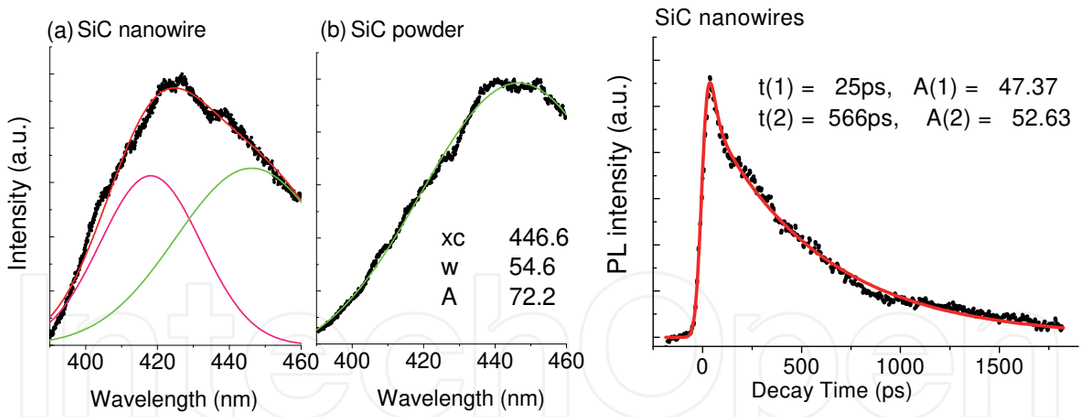

Fig. 7. Ultrafast light luminescence from nanowires and micro powder of SiC, (a) and (b) are the wavelength domain properties of nanowires and micro powder of SiC; (c) is the time domain curve of nanowires of SiC. All scatter dots are for the experimental results and the solid lines are the fitting results.

As the new peak at 418 nm is the dominant emission of the SiC nanowires, we will focus on its dynamic analysis. The red line in Fig. 7c shows the biexponential fitting result to the experimental data. The deconvolution result shows that the two decay constants of the SiC nanowires are 25 ps and 566 ps, respectively. It implies the coexistence of two different recombination paths. It should be noted that the decay time of 567 ps is on the same order of magnitude of that of the SiC nanocrystalline films reported and is nearly three orders of

magnitude faster than that of the bound-exciton transitions of bulk SiC at low temperature (Hartman and Dean, 1970). The other decay time is 26 ps. Since quantum confinement effects is indicated occur in low-dimensional SiC, the geometrical restriction of the electron-hole pairs lead to a strong enhancement effect of the oscillator strength of the confined levels resulting in direct transitions in the nanowires and the faster decay process.
Similar explanation has been proposed in low-dimensional Si to account for the fast decay process. Similar results of Si nanowires at room temperature have comparable PL decay time (20 ps), which is also attributed to the luminescence due to the quantum-confinement effect. On the other hand, it's known that surface states play an important role in the carrier recombination process with large surface-to-volume ratio in low-dimensional Si. Theoretical calculation shows that the lifetime of self-trapped exciton localized at the surface state is close to 1 ns. Furthermore, similar lifetime (~1 ns) has been found in low-dimensional Si and SiC experimentally, which is also attributed to the recombination of the excitons localized at the surface states. Thus, the slower decay process in SiC nanowires could be subjected to the surface states recombination process. This can be further proved by the energy dispersive x-ray analysis, which shows that the nanowires are pure, containing only Si and C indicating that the slower process is not possible from impurity related emission centers.
In summary, the needle-shaped SiC nanowires give intense blue light emission band peaking at 418 nm under UV fs laser excitation at room temperature. TRPL analysis result shows a biexponential decay behaviour with a faster time constant of 26 ps and a slower one of 567 ps, respectively. The faster decay component is attributed to the direct recombination of the quantum-confined carriers, while the slower one corresponding to the recombination of excitons localized at surface states.

2.3.2 Super fluorescence from nanowires of WO

The ultrafast light emission from WO nanowires is analyzed by two steps. First we have detected the time-wavelength-intensity dependent spectroscopy. Under femtosecond laser excitation the WO nanowires undergo two significant effects. One is the PL intensity increases dramatically as the pumping intensity increases. The other is the life-time was shortened to almost to the same level of the instrumental response. To make it quantitatively, we have carried the pump intensity dependent PL measurement which is shown in Fig. 8 (b). We can find that under the low intensity of the pumping, the PL intensity is proportional to the pumping intensity which means that PL emission comes from the spontaneous emission. We applied the linear fitting curve of the function of $I_e=a_1I_p$ (the red scatter data, a_1 is a constant of 6.0) and find that under the pumping power of 100M/cm^2, the linear fitting is quite accordant with the experiment. That is under such low excitation the PL comes from spontaneous emission dominantly. While for higher intensity of pumping, we can find that the PL-pumping relationship turns to be quadratic and the fitting curve of the function of $I_e=a_2I_p^2$ (the green dot line, a_2 is a constant of 0.28) matches the experimental results well with the only regret that not enough data points were obtained on the lack of intensity of the laser system. Such a quadratic relationship between the PL intensity and the excitation is one dominant factor for lasing effect. On the other hand we can get clear that the life-time is shorted dramatically from the spontaneous emission this is another factor for lasing effect of materials. But the bandwidth sharpening has not been detected under such a spectral resolution.

Another interesting result is that there is a band shift in Fig. 8 (a) when the pumping intensity increases the lasing like peak turns to shift to red. We applied the high spectral measurement to investigate the detail dynamics of the PL behaviour as shown in Figure 9. The left side in Figure is the integration of the whole image of the streak camera. As the spectral resolution improved the wavelength spectroscopy can be found that there be three bands from the wavelength from 385nm to 395nm corresponding to the transition of the oxygen vacancies. The bandgap of WO is 2.6~2.7 eV corresponding wavelength about 460nm. While the resonant states introduced by oxygen vacancies can generate an direct transition leading to photonic emission with much high efficiency than that of the intrinsic transition from the conduction band to the valence band because the WO is the indirect semiconductor (Karazhanov et al., 2003).

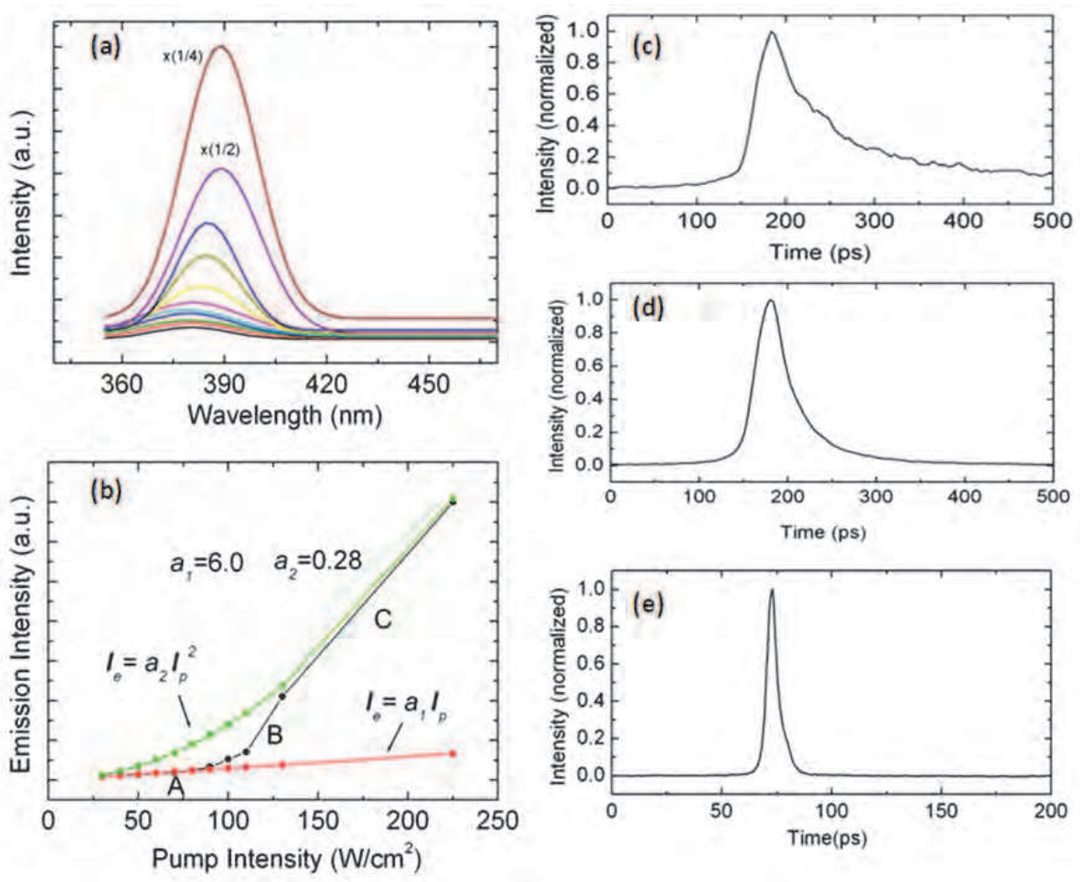

Fig. 8. (a) The emission intensity spectra of WO_{3-x} nanowires obtained under the pump intensities of femtosecond laser, correspondingly from low to high, of 30, 40, 50, 60, 70, 80, 90, 100, 110, 130, and 225 W/cm², respectively.（b）The intensity of emission peak versus the pump intensity (the black dot line), the fitting curve of the function of $I_e=a_1Ip$ (the red dot line, a1 is a constant of 6.0), and the fitting curve of the function of $I_e=a_2Ip^2$ (the green dot line, a2 is a constant of 0.28). (c), (d), and (e) are the emission decay curves of WO_{3-x} nanowires at low pump intensity of less than 90 W/cm²(section A), the midst pump density of 110 W/cm²((section B), and high pump density of more than 130 W/cm² (section C), respectively.

The most significant experimental finding of our study is the time-resolved spectroscopy measurement of SF which resolves in first time the dynamic process of a SF in picosecond-scale. As shown in Figs. 9(a) and 9(b), a red shift and a blue shift at the first and second halves of the SF pulse have been clearly detected, respectively, with use of high spectral resolution spectrometer (0.5 nm) and high time resolution of our streak camera (less than 1.0 ps). Three peaks with the centre wavelengths of 396nm (3.13 eV), 391nm (3.17 eV), and 386 nm (3.21 eV) (Fig. 9(c)) can be seen at the time of 4.3, 5.5 and 8.9 ps (Fig. 9(d)) after the initiation of excitation pulse, respectively. Fig. 9(d) reveals that for the majority of emitted photons, the first group is at the wavelength of 396 nm at time of 4.3ps, the second one at 391 nm at time of 5.5ps and the last one at 386 nm at time of 8.8ps. The peak at 391 nm may be attributed to the recombination of Frenkel excitons themselves, and the peaks at 396 and 386 nm are then a red shift and a blue shift at the first and second halves of the ultrafast photo luminescent pulse, respectively. This effect of frequency-shift during radiation is the fingerprint characteristic of cooperative emission in solid state, different from the case of atomic gas system.

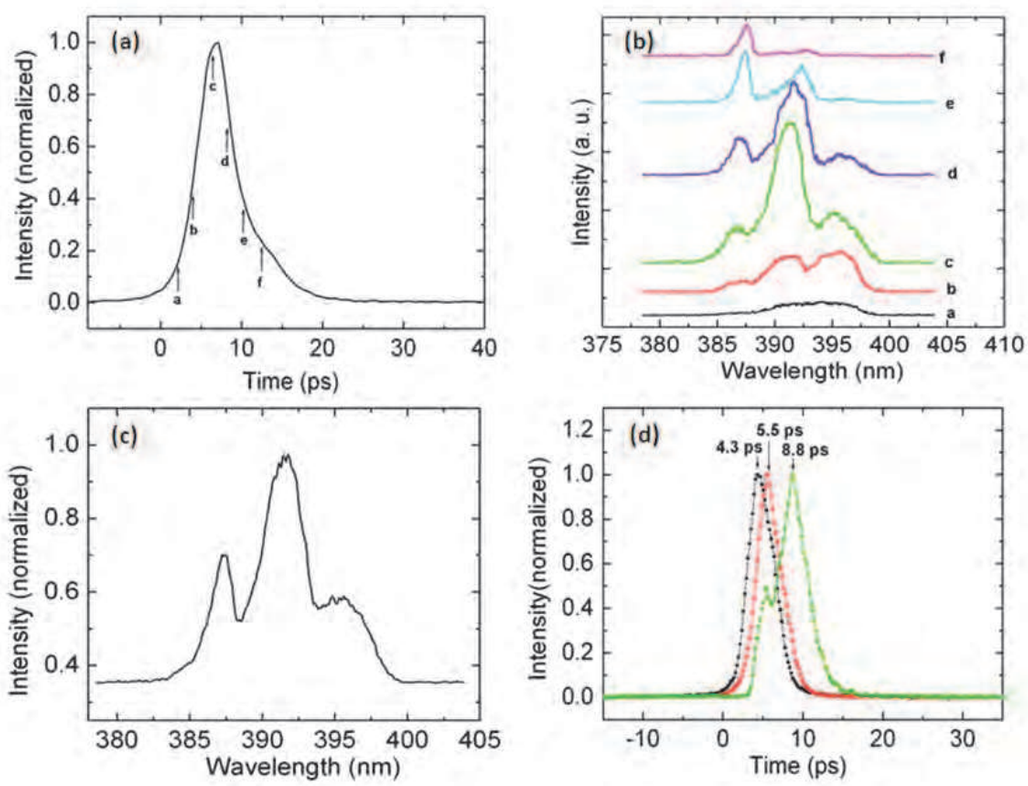

Fig. 9. (a) The ultraviolet SF pulse profile recorded under the pump intensity of 225 W/cm^2 (the peak of excitation pulse at the time of zero). (b) The time-resolved emission spectra of ultraviolet SF just recorded at the time of a, b, c, d, e, and f, which are indicated in (a). (c) The time-integrated spectrum of ultraviolet SF. (d) The emission decay curves of ultraviolet SF at the centre wavelength of 396 nm (black), 391 nm (red), and 386 nm (green); their maximal intensities occur at 4.3 ps, 5.5 ps and 8.8 ps after the peak of excitation pulse, respectively.

We have demonstrated a new new theoretical model for a two-dimensional system, and to apply it to explain the present findings (Luo et al. 2011).
As the theoretical model indicates that the first and last groups of emitted photons in SF process occur at $\hbar\omega_0 + 4\hbar\Omega$ and $\hbar\omega_0 - 4\hbar\Omega$ respectively which is independent on any N atoms system. It should be noted that the PL intensity is an ensemble emission from all nanowires with different large N atoms (oxygen vacancies) under illumination of the femtosecond laser beam. Thus, two strong peaks at $\hbar\omega_0 + 4\hbar\Omega$ and $\hbar\omega_0 - 4\hbar\Omega$ besides the strongest peak at $\hbar\omega_0$ should be observed in the time-integrated spectra as shown in Fig. 9(c). Furthermore, with assumption that the lattice constant of WO_3 cubic phase R_0 equals to 0.37 nm, the magnitude of the transition dipole of Frenkel exciton in WO nanowires is obtained as d = 4.25x10-30 m·C, which equals to the value of the dipole moment when the distance of an electron departure from the centre of positive charges is 0.265 Å (half of Bohr radius) which is quite a reasonable distance in practice.
Therefore ultrafast photo luminescent phenomena of various nanowires enrich the prospective application of nanowires in light sources and integrated photo electronics with both ideal structures of nanowires and the defects contained nanostructures. With the artificial nanostructures we can obtain various novel structures for further practical design of functional materials.

2.4 Directional lasing analysis form ZnO nanotrees

Compare with the uniform nanowires the composed structure of nanowires even with micro rods are a new kind of complex artificial materials with novel photo electronic features. Among various composed nano-micro structures ZnO nanotrees have attracted much attention in recent years. We have measured the ultrafast photo luminescent of ZnO nanotree with various spacial respects and found that there be different lasing behaviour inside the nanotree structures (Zhao et al., 2010).

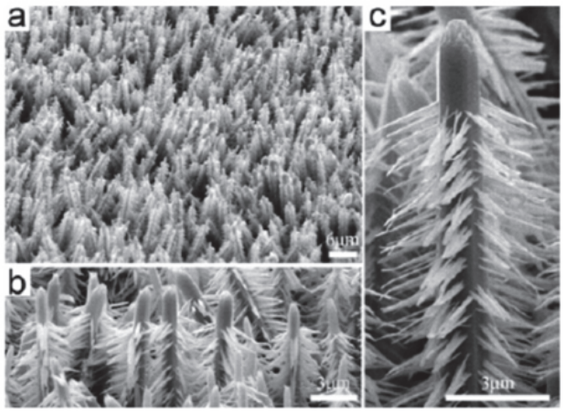

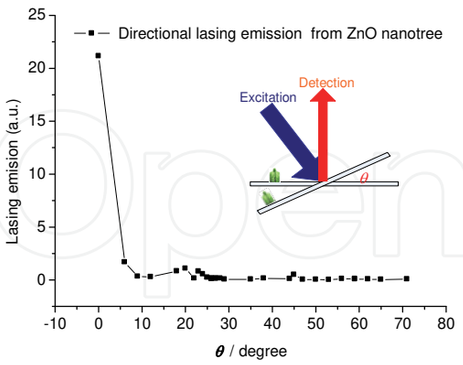

Fig. 10. SEM image of ZnO nanotree. a: title view; b: side view; c: magnification image of single nanotree. Fig. 11. Direction dependent lasing emission of ZnO nanotree structure.

From Figure 10 we can see clear that each ZnO nanotree is uniformly composed of a hexagonal prismatic microcrystalline trunk and radial-oriented nanobranches on the micro trunk's six columnar surfaces (Fig. 10 c), thus forming a nanostructured *pine tree forest* (Fig. 10, a-b). Time-resolved PL spectroscopy was demonstrated with a femtosecond optical

parameter amplification system (Spectra-Physics 800CF) as the excitation and a femtosecond synchroscan streak camera FESCA (HAMAMATSU C6860) connected with a spectroscope C5094 as the spectrum detecting system. The time resolution of the whole system is less than 1.0 picosecond and the best spectral resolution is 0.3 nm. The excitation femtosecond laser pulse was focused on the sample by a lens with focal length of 75 mm with both a sharp angle and a glance angle between the incident light and the normal of the sample plane respectively, the light emission from the sample was collected with a large NA lens with the focal length of 50 mm with lens radius of 50 mm. The composition of lenses was applied to generate a conjugated point of sample into the slit of spectroscope C5094 which connected by the streak camera modeled as FESCA C6860 triggered by the femtosecond laser oscillator at 82MHz. The OPA output was set at the wavelength of 320nm, with the pulse energy of 100 nano Joule per pulse. In order to change the excitation intensity we applied Glan-Laser Calcite Polarizer in front of the focusing lens of the sample. A short wavelength cut-off filter at 340nm was adjusted before the input slit of the spectroscope.

The spacial distribution of the ultrafast photoluminescence of ZnO tree was measured with the set-up as the schematic inset in Figure 11. As the trunk is parallel to the normal line of the sample plane we adjusted the angle between the excitation laser beam and the normal line of the sample to obtain the relationship between the lasing emission and the geometry of excitation to the nanotrees. The spacial intensity distribution shows the maximum lasing emission at the direction nearly parallel to the trunks which increase dramatically as the angle bends to nearly parallel to the direction of the trunk of the tree. This means no matter which direction to get the excitation the end effective lasing comes from the trunk of the nanotrees. Such effective lasing emission implies that there may be energy transfer process from the branches to the trunk of the nanotrees.

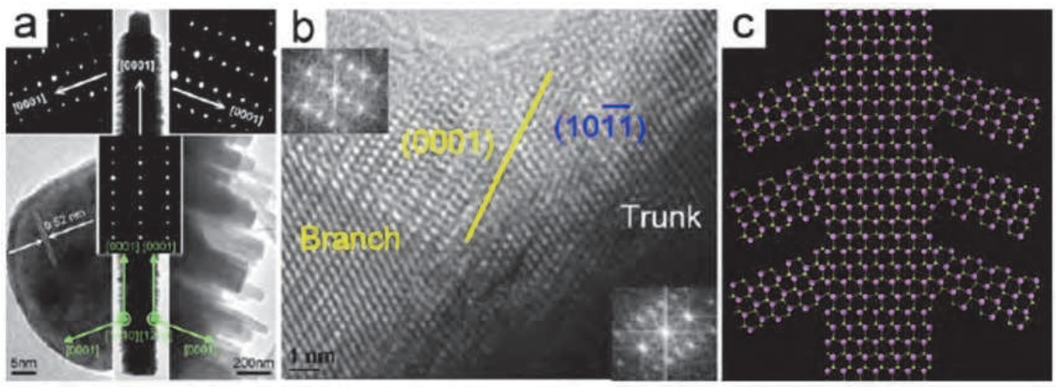

Fig. 12. XRD results of the ZnO nanotree, a: TEM image of nanotree, b: HRTEM of branch-trunk junction, c: schematic structure model of ZnO nanotree.

By checking the crystal structure of the ZnO nanotree we can find that both the microtrunks and the nanobranches have grown along the ***c*** axis (Fig. 12). All the microtrunks stand nearly vertical on the zinc substrate due probably to either the first few layers *in situ* formed on the Zn or the adsorbed *en's* interfacing. The smooth nanobranches, however, are not exactly perpendicular but oblique to the columnar surface of the microtrunk, with an angle of about 108° between growth direction of the branches and that of the microtrunk. Thus if the ***c*** axis is the proper lasing direction we should have detected the lasing effect at the angle along the nanobranches and trunks. There should be other behaviour dependent. We

applied the excitation with different orientations and the corresponding detection for both the microtrunks and the nanobranches.

As the nanotree shows a specific spatial construction compared with other homogeneous nanowires and nanorods we should explore the detailed light emission on the basis of the novel structures. In order to explore the details of the excitation energy flow we demonstrated four extremely schematic setups for the detection of the dynamic lasing emission. According to the directions of the excitation and detection, we denote the E for excitation and D for detection which addressed letter V for the nearly parallel to the ***c*** axis of the trunk and H for the line forming a large angle of 78° with the ***c*** axis of the trunk, respectively. In order to practical adjustment of all lens and apparatus, we have assigned the setup EVDV and EHDH by narrowing to a sharp angle of 15° as shown in Figure 13.

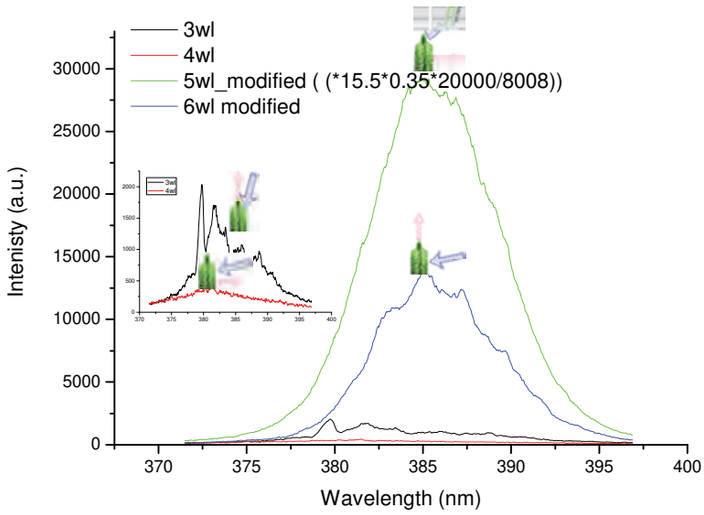

Fig. 13. Comparative lasing efficiency under different geometrical conditions. The blue arrow and the red arrow represent for the excitation and the emission correspondingly. The number is for modification in order to get proper ccomparisons among different conditions.

Figure 13 shows that when the excitation was set vertically, the lasing along the trunk presents in different separate modes. One of the most significant lasing comes from the mode at wavelength of 379 nm which was assigned as P band of ZnO nanostructures. The others separate modes should come from the cavity effect of the trunk. From the separation and the cavity analysis we can calculate the length trunk is about 15 micro meters long accordant with the morphology. But the horizontal light emission (EHDH) shows a wide band with very low intensity. Such ultrafast light emission is similar to amplified spontaneous emission. Furthermore, we can find that such light emission undergoes red-shift compared to that of trunk which is due to the nanostructures larger than 100nm scale. Therefore, we attribute such wide band random lasing to the light emission of the nanobranches growing on the trunk with angle of 108° to the ***c*** axis of the trunk.

Because the far field lasing emission are all demonstrated by the light with the polarization perpendicular to the ***c*** axis of the wurtzite structure of ZnO, while for the light emission from the direction of electric vector parallel to ***c*** axis has been vanished in far field detection. Therefore we turn to the component perpendicular to ***c*** axis of branches and trunk correspondingly. When the excitation beam was set at the sharp angle

(15°, EVDV), the projective factors of the electric components of the trunk and the branches are 0.966 and 0.052 respectively. While for the large angle excitation setup (78°, EHDV and EHDV), the excitation of the trunk has been decreased as the projective factor coming down to 0.208 and the branches excitation has been increased as the projective factor up to 0.866. Thus under semi-parallel setup the trunk got mainly excited and the lasing emission parallel to the trunk axis presents cavity modes significantly which is confirmed by our discussion above.

As for semi-perpendicular excitation (EH), we may expect that the branches get mainly excited and the trunk got excited much less than that of semi-parallel setup the light emission should be mainly from the branches of the nanotree. But the result has shown much different to such a deduction. Firstly, as the branches undergo the structure in nanometer scale, the light emission presents a wide band spectrum as detected under EHDH, but it demonstrated a very low intensity compared to the trunk emission of EVDV setup. Secondly, with the detection of EHDV separate modes are distinguished with the same wavelength separation as that of the EVDV as well as much higher intensity and a slight redshift than that of EVDV. Because the excitation keeps the same under these two conditions we should consider the energy transfer from the branches to the trunk of the nanotree. Since the PL only concerns about the electric vector perpendicular to the c axis the detected light emission far field is only the emission of the electric vector which is perpendicular to the corresponding ***c*** axis of the trunk and the branches. While for the connecting part of the trunk and branches there are structure defects there should be coupling between two directional electric vectors which dominating the energy transfer from the branches. As the interaction and energy dissipation of the energy processes there should be a redshift of the acceptor to the energy donor. Such a redshift matches the spectra from EVDV and EHDV.

As we known that photosynthesis is one of the most important energy transform process on earth and the initial energy transfer process is the key step to harvest the solar energy for the coming processes, the artificial ultrafast energy harvesting apparatus has attracted much more attention of both material experts and photonic scientists. Our nanotree of ZnO has the similar structure as the LHC of algae which has six antae linked onto the core structure. Since the core structure is arranged on the membrane of the thylakoid behaving as the acceptor of the excitation energy, this open a door for us to applied a certain structure to the trunk of the nano-pine-tree to link to the corresponding acceptor of such a coherent excitation leading to energy transferring apparatus with high efficiency and high speed.

The PL efficiency of trunk to branches has been calculated based on the structural statistics. Table 1 shows the detailed calculation of TB ratio (Data have been listed in Table 2.). The efficiency is the projection factor of the excitation beam. The structural T/B ration is the ratio of the absorption cross area based on the structural statistics. The experimental T/B ratio is calculated from the PL spectroscopy. Under the vertical excitation the structural T/B ratio is 0.355 while the experimental T/B ratio is 0.063 indicating that there is part of energy transferred from the trunk to the branches. But under parallel excitation, the structural T/B ratio is 0.496 while the experimental ratio is up to 20.6 showing that the majority of the excitation energy in the branches transferred into the trunk leading to a large PL ratio of T/B.

To study the dynamic process of the nanotree structures, we have carried out a excitation – dependent lasing detection, which under the parallel condition we adjusted the excitation

laser power by Glan-Laser Calcite Polarizer prism from few micro Watt to about 120 micro Watt. The excitation dependent lasing emission is shown in Figure 14. Figure 14 (a) is the time-decay curves of both lower excited lasing emission and the higher excited lasing emission respectively. The slower delay curve belongs to the lower excitation at the mean optical power of 5.5 micro Watt which corresponding to the focal pumping density of 374MW/cm^2. Such a process was taken to the ultrafast lasing emission of high excitation but not relates to the correlated light emission. The fast decay curve belongs to the higher pumping at the mean focal density of 3.4GW/cm^2, which is closed to bring the correlated light emission such that we have obtained the almost Gaussian profile of the delay curve which means that the light emission response time is less than the excitation lasing pulse, about 4 picoseconds in our experiment.

Furthermore, a clear linear relationship has been given by the intensities of both excitation and lasing emission as shown in Figure 14 (b). The fitting result shows that the threshold of excitation for lasing emission is 20 micro Watt. The linear dependence of the light emission with the intensity matches the laser theory of a constant gain efficiency of the gain medium which is nanostructures ZnO in our experiment. Therefore the trunk of the nanotree behaves as both the gain medium and the cavity of the lasing emission. The branches play the role of light harvesting and transfer the harvested energy to the laser cavity to get the phase matched lasing emission. Such a geometrical restricting lasing structure is appropriated for photo electronic integration.

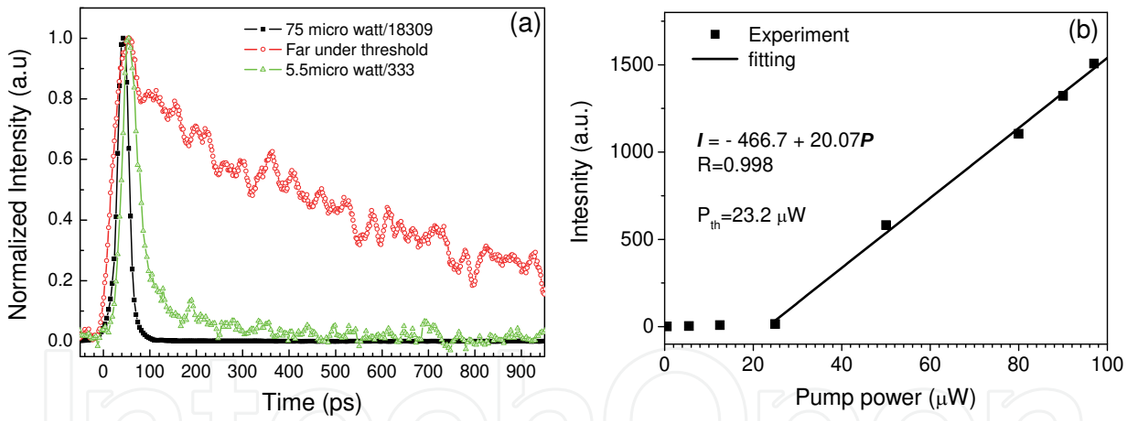

Fig. 14. Lasing effect of the nanotree under parallel excitation. a) Time-resolved spectra of emission under different pumping intensity. b) Dependence of light emission on the excitation intensity.

One important comment is that on order to get the lasing emission evidently we have carried all the lasing detection under the pumping laser intensity at the power of 50 micro Watt corresponding to the focal light intensity of 3.4 GW/cm^2. Additionally, for the more detailed dynamic energy transfer study we have demonstrated the ultrafast ling detection under the fastest responding selection but have not obtained any significant improved results. It implies that the energy transfer between the branches and the trunk must be much faster than 1.0 picosecond, the time-resolution of our detection system, which may have a certain degree of coherent interaction between the trunk and branches of the ZnO nanotree.

From discussion above, we have demonstrated a directional lasing emission from structured ZnO nanotree with ultrafast time-resolved laser spectroscopy. The lasing shows a far field diffraction angle less than 0.04 rad (Figure 11) with separate cavity modes. The detailed direction excitation setup analysis gives an ultrafast energy transfer between the branches and the trunk of the nanotree evidently. Nano branches play the role of light harvesting and transferring the harvested energy to the trunk which behaves as both the gain medium and the laser cavity for phase matching of lasing emission. Such a geometrical restricting lasing structure is appropriated for photo electronic integration (Wang et al., 2009). The transferring time may be much faster than 1.0 picosecond. The results imply that with proper artificial techniques man can fabricate apparatus with featured high energy transfer function and ultrafast energy transfer time as well as high intensity lasing emission shedding light on the ultrahigh speed light communications and integrated photo electronic.

Ex	Em	Excitation efficiency	Trunk area	power	Branch area	power	Experimental detection	
			T	T	B	B	T	B
V	H	0.0955	0.335	0.021	0.665	0.064		270490
	V	0.9045	0.264	0.239	0.736	0.667	16958	
				0.260		0.732		
T/B ratio			0.355				0.063	
H	H	0.9568	0.335	0.320	0.665	0.636		5656
	V	0.0432	0.264	0.011	0.736	0.032	116700	
				0.331		0.668		
T/B ratio			0.496				20.6	

Table 2. The energy transfer calculation between the trunks and the branches of the ZnO nanotrees, Ex is for the excitation direction while Em for the detection direction.

3. Conclusion

In summary, nanowires as one-dimensional material have attracted much attention on the functional application research. Photo electronic properties determine its application on photo detection, integrated optical devices and novel kinds of light source.

We have constructed a series experiments for the ultrafast photo luminescence detection and completed the analysis of the mechanisms of the ultrafast light emission from various nanowires as well as beginning with the nanoparticles of ZnO. We have found the surface state induced ultrafast light emission from the transition within the bandgap in ZnO nanoparticles and measured that there is a size threshold for surface state induced light emission. Besides, we have detected the ultrafast blue light emission from the needle like SiC nanowires and the spectral results show the significant quantum confinement. Furthermore, we have accomplished the mechanism studies on the super fluorescence from WO nanowires and concluded that the SF is due to the oxygen defects resonance transition. To investigate the nanowires UPL more practically, we developed a complex set-up to study the ultrafast light emission of the nanotrees of ZnO and find the lasing

effect from the trunks of the nanotrees and find the clue of the energy transfer from the branches to the trunks. From the ultrafast photo luminescence studies we have been clear for the following.

With proper artificial design man can find the wide-band ultrafast light emission due to the surface-state. Because the bandwidth of surface state induced light emission can be tuned through the size of the material in nanometre scale we may construct optional light sources by the size design. Certainly surface state can also bring trouble for the neat narrow band emission this should be pay attention in the material design.

The super fluorescence in the defect contained nanowires made of indirect semiconductors such as WO nanowires brings new hope for ultrafast integrated photo electronics. Several picoseconds response time means an ultrafast light transformation in practice.

Composition of the nanotree undergoes the ultrafast lasing effect and energy transfer phenomenon. Such structure may be useful for artificial solar energy harvesting apparatus development.

4. Acknowledgment

The authors gratefully acknowledge the financial support of the project from the National Natural Science Foundation of China (Grant No. 10574165), the project from the Natural Science Foundation of Guangdong (Grant No. 8151027501000017), the Science and Technology Department of Guangdong Province, the Department of Information Industry of Guangdong Province and the Science and Technology Department of Guangzhou City.

5. References

Bimberg, D., Skolnick, M.S., Choyke, W.J., 1978. Observation of an Electron-Hole Liquid in Cubic SiC. Physical Review Letters 40, 56.

Djurisic, A.B., Kwok, W.M., Leung, Y.H., Phillips, D.L., Chan, W.K., 2005. Stimulated emission in ZnO nanostructures: A time-resolved study. J. Phys. Chem. B 109, 19228-19233.

Hartman, R.L., Dean, P.J., 1970. Magneto-Optical Properties and Recombination Rate of the Green Luminescence in Cubic SiC. Phys. Rev. B 2, 951.

Luo, J.Y., Xu, N.S., Zhao, F.L., Deng, S.Z., Tao, Y.T., 2011. Ultraviolet superfluorescence from oxygen vacancies in WO3-x nanowires at room temperature. J. Appl. Phys 109, 024312.

Karazhanov, S.Z., Zhang, Y., Wang, L.W., Mascarenhas, A., Deb, S., 2003. Resonant defect states and strong lattice relaxation of oxygen vacancies in WO_{3}. Phys. Rev. B 68, 233204.

Wang, X.F., Xie, P.B., Zhao, F.L., Wang, H.Z., Wang, Y.M., 2009. Spectra of ZnO nanoparticles under low photon energy excitation. Particuology 7, 496-500.

Wang, X.F., Zhao, F.L., Xie, P.B., Deng, S.Z., Xu, N.S., Wang, H.Z., 2006. Surface emission characteristics of ZnO nanoparticles. Chem. Phys. Lett. 423, 361-365.

Wang, X.F., Zhao, F.L., Xie, P.B., Liang, S.D., Wang, X.F., Xu, N.S., 2007. Surface luminescence in ZnO nanoparticles. Optics Communications 276, 186-190.

Zhao, F.H., Zheng, J.G., Yang, X.F., Li, X.Y., Wang, J., Zhao, F.L., Wong, K.S., Liang, C.L., Wu, M.M., 2010. Complex ZnO nanotree arrays with tunable top, stem and branch structures. Nanoscale 2, 1674-1683.

Zhao, F.L., Chen, H.X., Deng, S.Z., Xu, N.S., Jia, T.Q., Xu, Z.Z., 2007. Ultrafast blue light emission from SiC nanowires. Chinese Optics Letters 5, 184-186.

Zhao, F.L., Gong, Z., Liang, S.D., Xu, N.S., Deng, S.Z., Chen, J., Wang, H.Z., 2004. Ultrafast optical emission of nanodiamond induced by laser excitation. Appl. Phys. Lett. 85, 914-916.

Nanowires - Implementations and Applications

Edited by Dr. Abbass Hashim

ISBN 978-953-307-318-7
Hard cover, 538 pages
Publisher InTech
Published online 18, July, 2011
Published in print edition July, 2011

This potentially unique work offers various approaches on the implementation of nanowires. As it is widely known, nanotechnology presents the control of matter at the nanoscale and nanodimensions within few nanometers, whereas this exclusive phenomenon enables us to determine novel applications. This book presents an overview of recent and current nanowire application and implementation research worldwide. We examine methods of nanowire synthesis, types of materials used, and applications associated with nanowire research. Wide surveys of global activities in nanowire research are presented, as well.

How to reference

In order to correctly reference this scholarly work, feel free to copy and paste the following:

Fuli Zhao, Xiaofang Wang, Huanjun Chen and Jianyi Luo (2011). Photoluminescence of Nanowires under Ultrashort Laser Pulse Excitation, Nanowires - Implementations and Applications, Dr. Abbass Hashim (Ed.), ISBN: 978-953-307-318-7, InTech, Available from: http://www.intechopen.com/books/nanowires-implementations-and-applications/photoluminescence-of-nanowires-under-ultrashort-laser-pulse-excitation

INTECH
open science | open minds

InTech Europe
University Campus STeP Ri
Slavka Krautzeka 83/A
51000 Rijeka, Croatia
Phone: +385 (51) 770 447
Fax: +385 (51) 686 166
www.intechopen.com

InTech China
Unit 405, Office Block, Hotel Equatorial Shanghai
No.65, Yan An Road (West), Shanghai, 200040, China
中国上海市延安西路65号上海国际贵都大饭店办公楼405单元
Phone: +86-21-62489820
Fax: +86-21-62489821

IntechOpen